Accepted Manuscript

Cell Culture System for Analysis of Genetic Heterogeneity Within Hepatocellular Carcinomas and Response to Pharmacologic Agents

Qiang Gao, Zhi-Chao Wang, Meng Duan, Yi-Hui Lin, Xue-Ya Zhou, Daniel L. Worthley, Xiao-Ying Wang, Gang Niu, Yuchao Xia, Minghua Deng, Long-Zi Liu, Jie-Yi Shi, Liu-Xiao Yang, Shu Zhang, Zhen-Bin Ding, Jian Zhou, Chun-Min Liang, Ya Cao, Lei Xiong, Ruibin Xi, Yong-Yong Shi, Jia Fan

PII: S0016-5085(16)35033-8
DOI: 10.1053/j.gastro.2016.09.008
Reference: YGAST 60684

To appear in: *Gastroenterology*
Accepted Date: 4 September 2016

Please cite this article as: Gao Q, Wang Z-C, Duan M, Lin Y-H, Zhou X-Y, Worthley DL, Wang X-Y, Niu G, Xia Y, Deng M, Liu L-Z, Shi J-Y, Yang L-X, Zhang S, Ding Z-B, Zhou J, Liang C-M, Cao Y, Xiong L, Xi R, Shi Y-Y, Fan J, Cell Culture System for Analysis of Genetic Heterogeneity Within Hepatocellular Carcinomas and Response to Pharmacologic Agents, *Gastroenterology* (2016), doi: 10.1053/j.gastro.2016.09.008.

Cell Culture System for Analysis of Genetic Heterogeneity Within Hepatocellular Carcinomas and Response to Pharmacologic Agents

Qiang Gao[1†], Zhi-Chao Wang[1†], Meng Duan[1†], Yi-Hui Lin[2], Xue-Ya Zhou[3], Daniel L Worthley[4], Xiao-Ying Wang[1], Gang Niu[2], Yuchao Xia[5], Minghua Deng[5], Long-Zi Liu[1], Jie-Yi Shi[1], Liu-Xiao Yang[1], Shu Zhang[1], Zhen-Bin Ding[1], Jian Zhou[1,6],Chun-Min Liang[7], Ya Cao[8], Lei Xiong[2], Ruibin Xi[5],Yong-Yong Shi[9], and Jia Fan[1,6]

Authors' Affiliations:

[1] Liver Cancer Institute, Zhongshan Hospital, and Key Laboratory of Carcinogenesis and Cancer Invasion (Ministry of Education), Fudan University, Shanghai, China

[2] Institute of Precision Medicine, 3D Medicines Inc., Shanghai, China

[3] Department of Psychiatry, Li Ka Shing Faculty of Medicine, the University of Hong Kong, Pokfulam, Hong Kong SAR, China

[4] Cancer Theme, SAHMRI and Department of Medicine, University of Adelaide, Adelaide, Australia

[5] School of Mathematical Sciences and Center for Statistical Science, Peking University, Beijing, China

[6] Cancer Center, Institute of Biomedical Sciences, Fudan University, Shanghai, China

[7] Department of Anatomy and Histology and Embryology, Shanghai Medical College, Fudan University, Shanghai, China

[8] Cancer Research Institute, Xiangya School of Medicine, Central South University, Hunan, China

[9] Bio-X Institutes, Key Laboratory for the Genetics of Developmental and Neuropsychiatric Disorders (Ministry of Education), Shanghai Jiao Tong University, Shanghai, China

[†] These authors contributed equally to this work.

Short Title: Attack Intratumor Heterogeneity in HCC

Grant Support: This work was supported by the National Key Sci-Tech Project of China (2013ZX10002010), National Natural Science Foundation of China (Nos. 81522036, 81572292, 81372648, 81272725 & 71532001), National Program for Special Support of Eminent Professionals (for Q.G.), Shanghai "Promising Youth Medical Worker" Project (No. 13Y055) and National Key Basic Research Program of China (No. 2015CB856000).

Abbreviations: HCC, hepatocellular carcinoma; ITH, intratumor heterogeneity; PDPC, patient-derived primary cancer cell; WES, whole-exome sequencing; HBV, hepatitis B virus; indels, insertions or deletions; AFP, α-fetoprotein.

Corresponding Authors: Jia Fan, Liver Cancer Institute, Zhongshan Hospital, Fudan University, 180 Fenglin Road, Shanghai 200032, China. Tel/Fax: +86-21-64037181; E-mail: fan.jia@zs-hospital.sh.cn; or Yong-Yong Shi, Bio-X Institutes, Key Laboratory for the Genetics of Developmental and Neuropsychiatric Disorders (Ministry of Education), Shanghai Jiao Tong University, Shanghai, China, Tel/Fax: +86-21-62932151;

E-mail: shiyongyong@gmail.com.

Disclosures: The authors declare no conflicts of interest.

Author Contributions: Q.G., Y.Y.S. and J.F. designed the study and directed the entire study. L. X., Y.C., and J. Z. participated in the study design. Q.G., G.N., X.Y.Z., M.D., and Y.X. performed analyses of sequencing data. Q.G., M.D., Z.C.W., X.Y.W., and J.Y.S., performed in vitro experiments. L.X.Y., G.N., and X.Y.Z. performed copy number analysis. Y.Y.S., L.Z.L., S.Z., and R.X. performed statistical analyses. J.Z., X.Y.W., and J.F. provided samples and clinical data. J.F., J. Z., and C.M.L. supervised the diagnosis of patients and subject recruitment. Q.G., Y.Y.S. and J.F. wrote the manuscript. D.L.W. critically reviewed the manuscript. All authors reviewed and approved the final manuscript.

ABSTRACT

BACKGROUND & AIMS: No targeted therapies have been found to be effective against hepatocellular carcinoma (HCC), possibly due to the large degree of intratumor heterogeneity. We performed genetic analyses of different regions of HCCs to evaluate levels of intratumor heterogeneity and associate alterations with responses to different pharmacologic agents.

METHODS: We obtained samples of HCCs (associated with hepatitis B virus infection) from 10 patients undergoing curative resection, before adjuvant therapy, at hospitals in China. We collected 4–9 spatially distinct samples from each tumor (55 regions total), performed histologic analyses, isolated cancer cells, and carried them low-passage culture. We performed whole-exome sequencing, copy-number analysis and high-throughput screening of the cultured primary cancer cells. We tested responses of an additional 105 liver cancer cell lines to a FGFR4 inhibitor.

RESULTS: We identified a total of 3670 non-silent mutations (3192 missense, 94 splice-site variants, and 222 indels) in the tumor samples. We observed considerable intratumor heterogeneity and branched evolution in all 10 tumors; the average percentage of heterogeneous mutations in each tumor was 39.7% (range, 12.9%–68.5%). We found significant mutation shifts toward C>T and C>G substitutions in branches of phylogenetic trees among samples from each tumor ($P < .0001$). Of note, 14 of the 26 oncogenic alterations (53.8%) varied among subclones that mapped to different branches. Genetic alterations that can be targeted by existing pharmacologic agents (such as those in *FGF19, DDR2, PDGFRA* and *TOP1*) were identified in intratumor subregions from 4 HCCs and were associated with sensitivity to these agents. However, cells from the

remaining subregions, which did not have these alterations, were not sensitive to these drugs. High-throughput screening identified pharmacologic agents to which these cells were sensitive, however. Overexpression of FGF19 correlated with sensitivity of cells to an inhibitor of FGFR4; this observation was validated in 105 liver cancer cell lines (*P*=.0024).

CONCLUSIONS: By analyzing genetic alterations in different tumor regions of 10 HCCs, we observed extensive intratumor heterogeneity. Our patient-derived cell line-based model, integrating genetic and pharmacologic data from multi-regional cancer samples, provides a platform to elucidate how intratumor heterogeneity affects sensitivity to different therapeutic agents.

KEY WORDS: Liver cancer; next-generation sequencing; patient-derived cell lines; targeted therapy.

INTRODUCTION

Hepatocellular carcinoma (HCC) is the second leading cause of cancer deaths with increasing incidence and mortality worldwide.[1] Most HCC patients are diagnosed at intermediate or advanced stages, making them ineligible for curative therapy.[2] In the era of precision medicine, molecularly targeted therapy has improved clinical outcome in many cancer types. In contrast, targeted therapy has so far been dismal in HCC, and only sorafenib could improve overall survival by a median of 3 months.[3] After sorafenib, up to seven randomized phase III clinical trials investigating other molecularly targeted therapies in HCC have reported negative results. Among other potential reasons, intratumor heterogeneity (ITH) has been proposed as a major obstacle for effective drug development in HCC.[3]

Recently, multi-regional deep-sequencing on tumor tissues has revealed considerable ITH with substantial prognostic, therapeutic and biological implications for many human cancers.[4-7] In HCC, although deep-sequencing has been applied on over 1,000 patient samples, uncovering a group of driver genetic alterations,[8-13] the landscape of spatial and temporal ITH remains elusive. Moreover, whether ITH in HCC patients is driven by different driver alterations, which requires different treatments, or alternatively ITH only reflects passenger changes without significant impact on drug-specific responses remain elusive. Simultaneous genetic profiling of and pharmacological testing on multi-regional tumor cells is a straightforward approach to figure out how ITH impacts on drug sensitivity. However, such hypothesis cannot be directly tested on the nonviable tumor tissues. It is noteworthy that patient-derived primary cancer cells (PDPCs) obtained by single sampling were innovatively used for drug discovery to overcome resistance in lung

cancer.[14] Therefore, PDPCs are not only attractive for testing drug response, but also preferable for genomic sequencing, given their population purity and stability.

To give a comprehensive view of intratumor genomic diversity and evaluate how the ITH can influence therapeutic responses in HCC, we combined multi-regional sampling, primary culture, genomic profiling and pharmacological screening in 10 resected HBV-related HCCs. We established a multi-regional cell culture model derived from geographical sampling of different intratumor regions that integrates cancer genetics with pharmacologic interrogation. This strategy provides a pipeline for the discovery and validation of clinically relevant precise therapy for HCC.

PATIENTS AND METHODS

Patients and Sample Collection

To investigate ITH, samples were collected from 10 patients diagnosed with HBV-related HCC who underwent curative resection prior to any adjuvant therapy **(Figure 1A and Supplementary Table 1**). The primary tumors were evenly sliced to pieces and spatially separated samples from each cut face were obtained immediately after resection. Representative spatially separated regions of each tumor were sent for H&E staining and primary culture. Typically, the culture took one month to establish low-passage PDPCs, which were further subjected to genetic and pharmacologic evaluations. The study was approved by the Research Ethics Committee of Zhongshan Hospital with written informed consent from each patient.

Whole-Exome Sequencing (WES), Mutation calling, HBV integration and Sanger

Validation

Genomic DNA was extracted from PDPCs, matched tissue and blood samples from the 10 HCC patients using DNeasy kit (Qiagen). WES of DNA samples was captured by Agilent SureSelect Human All Exon V4 kits and sequenced using Illumina HiSeq 2000 system. Paired-end sequencing (2 × 101 bp) was carried out using standard Illumina protocols. WES, Mutation calling, HBV integration detection and Sanger validation are detailed in **Supplementary** method.

Phylogenetic and Mutation Spectrum Analyses

Binary distributions of mutations were used to reconstruct the maximum parsimonious phylogenetic tree using Wagner method implemented in Penny of PHYLIP package.[5] The difference of mutation spectrum was examined in the distribution of trunks and non-trunks. P values of each mutation type were corrected for multiple testing by the Benjamini-Hochberg method.[4] Details of these analyses are described in **Supplementary** method.

Copy Number Alterations

DNA was processed and hybridized to Affymetrix CytoScan® HD array according to the manufacturer's protocol and described in **Supplementary** method. Quality control, gender verification, signal normalization and segmentation were conducted. The absolute copy numbers are inferred based on the extrapolation algorithm of TAPS.

Drug Screening, Real-Time RT-PCR and Immunoblotting Assays

The compounds and PCR primers used are listed in **Supplementary Tables 3 and 4** respectively. Details of the experimental procedures are described in **Supplementary** method.

Cell Lines for Testing FGFR inhibitor

A total of 105 liver cancer cell lines, independent of the 10 patients used for evaluating ITH, were used to test the sensitivity of FGFR inhibitor. The 105 lines consisted of 83 in-house established lines and 22 commercially available lines **(Supplementary Table 2)**. In total, 83 liver cancer cell lines were established in our lab, authenticated and employed for drug testing. Each cell line was derived from one HCC patient and cultured for at least 30-50 passages. The 22 commercial liver cancer cell lines were grown in recommended media and authenticated by STR analysis.

Statistical Analysis

Statistical analysis was performed using SPSS 19.0 (SPSS, IBM), except where specifically indicated. Data were presented as the means ± standard deviation. The χ^2 test, Fisher's exact test, Students' *t* test and Mann-Whitney *U* test were used as appropriate. Two-tailed P value < 0.05 indicates statistical significance.

RESULTS

Establishment of Multi-regional PDPCs from HCC Specimens

To illustrate ITH in HCC, we collected fresh tissues from 55 spatially distinct tumor regions (ranging of 4-9 per case) in 10 resected HBV-related HCC. The 10 patients with

stages T1 (n=4), T2 (n=5) and T3 (n=1) were treatment naive before operation (**Supplementary Table 1**). To test the sensitivity of these tumor cells to targeted therapeutics, we developed a short-term primary culture protocol that was amenable to high-throughput screening. Each tumor region was subjected to primary culture, followed by WES, CytoScan® HD Array and high-throughput screening (**Figure 1A**). WES was performed at mean depth of 89.0× (58-125.8 ± 12.5) on those 55 PDPCs (**Supplementary Table 5**). Due to culture enrichment, analyzing the tumor cell purity of low-passage PDPCs base on WES data revealed a mean of 98.6% (range of 88.1%-100%) purity, with 46 out of the 55 cell lines above 99%. The results were confirmed by immunohistochemical staining of a panel of HCC-related biomarkers, including serum α-fetoprotein (AFP), pan-CK, Hepar-1, α-SAM and Vimentin, on serial passaging, which also showed that our PDPCs were almost 100% cancer cells (data not shown). The average ploidy of those PDPCs was 3.20, ranging from 2.00-4.48 (**Supplementary Figure 1**), consistent with previous reports in HCC.[8, 10, 13] Totally, we identified 3,670 non-silent mutations, including 3,192 missense, 94 splice-site variants, and 222 indels (**Supplementary Table 6**). The median number of non-silent mutations was 93 per tumor, comparable to the results in three previous reports using single-biopsy HCC samples (67, 85, and 58 respectively; **Supplementary Figure 2**). We confirmed 92.2% of the 881 randomly selected non-silent mutations by Sanger sequencing (**Supplementary Table 7**).

Intratumor Heterogeneity and Clonal Evolution of HCC

To illustrate the extent of spatial and temporal ITH in HCC, phylogenetic trees based on non-silent somatic mutations of the 55 PDPCs were constructed for each of the 10

tumors. Each tree contains trunk, branches and private brunches. The trunk represents mutations shared in all regions, branch stands for heterogeneous mutations that present in at least 2 regions, and private brunch represents mutations only identified in one region in an individual tumor (**Supplementary Figure 3**).[4, 5] Notably, all the 10 tumors displayed clear evidence of branched evolution and intratumor mutational heterogeneity (**Figure 1B**). The average percentage of heterogeneous mutations (branch and private) was 39.7% (range of 12.9%-68.5%) (**Figure 2A**). This was substantially higher than the ITH measured by 1 or 2 gene mutation as reported in a recent study where a heterogeneous intratumor mutational status of *TP53* and *CTNNB1* were found in 22% of HCC.[15] Next, we focused on and characterized the genes that were reported to be recurrently altered in HCC, possibly acting as the driver genes.[8-13] In the 10 HCCs, a total of 26 such kind of driver genes were identified (including 7 amplified or deleted genes as discussed below) (**Supplementary Table 8**). We further mapped the 26 drivers to each phylogenetic tree and found that less than half of the driver alterations were trunk events that occurred early during HCC evolution (**Figure 1B**). Of note, 14 (53.8%) drivers were subclonal that mapped to branches in 8 out of the 10 cases, highlighting the need to target tumor subclonal compositions. *TERT* promoter mutations, one of the earliest genetic alterations in HCC,[16] were detected as trunk event in 5 cases and as branch event in one case. *TP53*, the top gene among the coding mutations in HCC, was mutated in all the 10 HCCs with various mutation types (**Figure 1B** and **Supplementary Table 6**). For example, cases 554, 703, 893 and 1900 harbored the R249S mutation which was typical of HBV-related HCC affected by aflatoxin B1.[17] Cases 307, 1026 and 1233 had stop-gained mutation (E300X), splicing mutation, and frameshift deletion (aa 202-206) respectively. Considering that

TP53 mutations occurred in about 27% of all HCC population and were most prevalent in HBV-related HCC,[8-13] the 10 cases examined here may represent a *TP53*-mutated subgroup of HCC related to HBV infection.

HBV integration is a well-known casual event during hepatocarcinogenesis. Based on the WES data, we identified 2 candidate HBV integration sites from cases 213 and 1900 **(Supplementary Figure 4)**. These two integration sites were both located at the promoter region of the *TERT* gene, which was shown to be the most prevalent gene integrated by HBV in HCC.[18] For both of the two patients, the breakpoints in the HBV genome were located at the gene X, consistent with the previous findings.[18] For case 213, 5 of the 5 tumor regions had the exact same integration site, indicating that HBV integration event was an early driving event. In case 1900, we only identified one tumor region (R4) having the integration at *TERT* promoter, possibly due to ITH or the limitations of WES that primarily cover the coding sequences.

We also investigated somatic copy number aberrations by CytoScan® HD array in the 55 PDPCs. Similar to the findings in lung and breast cancers,[5, 19] there were no obvious differences in large-scale chromosome alterations, and the log2 ratio profiling highly resembled among distinct regions from individual tumors (**Supplementary Figure 5**). Examining the altered small segments identified heterogeneous distribution within each tumor, including segments containing 7 potential driver genes (*FCRL1*, *DDR2*, *CCND1*, *FGF19*, *BRD7*, *ADH1B* and *CDKN2A*) (**Supplementary Figure 6**). The 7 potential drivers with amplification or deletion were mapped to the phylogenetic trees, with *CDKN2A* deletion in the trunk and the remaining 6 genes in the branches (**Figure 1B**).

Mutation Spectra of Trunk and Branch Mutations

We further analyzed the mutation spectra of the 10 HCCs. In all the 10 tumors (combining trunk and non-trunk), C>A transversion and C>T and T>C transitions were the predominant changes (**Figure 2B-C**). C>T transition is prevalent in many cancers,[4, 5] while C>A and T>C changes are considered as the characteristic signatures of HCC genome.[8-13] These results supported the notion that our PDPCs inherited the mutation patterns from original HCC tissues. Moreover, the proportions of C>T transition and C>G transversion increased dramatically in non-trunk in all 10 tumors either when considered in a combined fashion (q = 0.00012 and 0.0132 respectively, **Figure 2B**) or individually (**Figure 2C**). This pattern of mutation shift was prevalent in many human cancer types,[4, 5] implying a common feature of cancer evolution. Data have accumulating that APOBEC cytosine deaminase activity is a major source for C>T and C>G mutations that fuels intratumor genetic heterogeneity.[20] However, no association between the mutation shift and APOBEC activity was detected, indicating that APOBEC-catalyzed deamination was not the main source of DNA damage in this subgroup of HBV-related HCC.

Moreover, hierarchical clustering by mutation spectra classified the 10 HCCs into two groups (**Figure 2D**). Analyzing the relationship of clinicopathologic features between the two groups, like serum AFP level, tumor size, tumor differentiation, microscopic vascular invasion and tumor stage was then made. Only serum AFP level showed significant difference between groups I versus II (P = .016 for trunk grouping; **Figure 2E**). This may have important clinical implications, given that AFP is a diagnostic and prognostic biomarker for HCC.

Identification of Combination Therapies Based on Genetic Analysis and Pharmacologic Evaluation

The impact of ITH on drug response could not be directly tested on clinical samples. Our multi-regional PDPC model provided an opportunity to evaluate this effect. We first tested the first-in class drugs (sorafenib and oxaliplatin) of HCC in those 55 regional PDPCs. However, no PDPCs showed sensitivity to sorafenib or oxaliplatin (**Supplementary Figure 7**). The suggested genomic biomarkers (like *ARAF* mutations, and *VEGFA* or *FGF3/FGF4* amplifications, etc.) [21-23] for sorafenib sensitivity were absent in the 55 PDPCs. The resistance to the first-in class drugs prompted us to focus on the cases with druggable genetic alterations. Although previous HCC sequencing data have revealed limited druggable alterations, we indeed detected such druggable changes in 2 of 10 HCCs (20%). However, unlike lung cancer where most known druggable changes occur early in tumor evolution, we observed that our HCC druggable alterations only occurred in subclonal groups (brunches and private brunches), including *FGF19* amplification in case 307 and *DDR2* amplification in case 703.

Case 307 harbored *FGF19* amplification in R4, R5, R6, R8, R9, R10 and R12, but not in R1 and R3 (**Figure 1B** and **Supplementary Figure 8**). Since *FGF19* amplification is a putative driver in HCC[9-11] and a potential biomarker for FGFR inhibitors[13, 24], the pan-FGFRs (FGFR1-4) inhibitor LY2874455 was applied to those 9 regional PDPCs without abnormalities in FGFRs. Only R6, R10 and R12 were sensitive to LY2874455, while *FGF19* amplified R4, R5, R8 and R9 showed resistant pattern alike unamplified R1 and R3 (**Figure 3A**, left panel). The mRNA levels of FGF19 were then examined in those PDPCs (**Figure 3A**, middle panel) and the resistant regions uniformly showed

low/middle expression of FGF19, regardless of amplification or not, while the sensitive regions had consistently high FGF19 mRNA levels (**Figure 3A**, right panel). IC50s of FGF19 high expression group significantly differed with low/middle groups ($P < 0.01$; **Figure 3A**, right panel). The concentrations to inhibit FGFR and ERK phosphorylation were much lower in the FGF19-high group than that in the FGF19-low/middle groups (30 nM vs 300 nM or higher) (**Supplementary Figure 9**). Overall, in case 307, despite 64.7% ITH (56.4% ITH in sensitive group), "biomarker-oriented heterogeneity" (i.e., FGF19 overexpression) determined the sensitivity to predicted targeted therapeutics (**Figure 3B**). Furthermore, another 105 independent liver cancer cell lines (22 commercial lines and 83 lines established in house), the largest panel of liver cancer lines hitherto, were classified into high versus low/middle groups according to FGF19 mRNA levels **(Supplementary Table 2**). It was revealed that IC50s in FGF19-high group were dramatically lower than that in low/middle groups ($P = .0024$) (**Figure 3C**), authenticating the findings in case 307. Since the 6 resistant PDPCs in case 307 harbored no actionable variants, we then screened them with in-house compound library (**Supplementary Table 3**). Indeed, they were found to be responsive to JQ-1 (BRD4 inhibitor), elesclomol (HSP70 inhibitor), etc. (**Figure 3D**), implying potential combination therapies for this patient.

To further evaluate the effect of such combinational treatment, LY2874455 and JQ-1 were added to the cell mixture of FGF19 high and low expression PDPCs from case 307. The FGF19 high expression cells were labeled with Qtracker 605 (pink) and total cells were stained by Hoechst 33342 (blue). The co-treatment of the two compound led to the maximal reduction in cell population compared to those treated with either compound alone (24.6% vs 58.7% or 37.0%, on day 3) **(Figure 3E)**. The population change of

LY2874455 sensitive cells (FGF19 high expression, labeled in pink) was examined during the treatment. Compared to DMSO control, the percentage of FGF19-high cells dramatically decreased on days 3 and 4 with 100 nM LY2874455 treatment, but showed no significant changes when co-treated with 100 nM LY2874455 and 1 μM JQ1, whereas remarkably increased with 1 μM JQ1 treatment, despite the reduction of total cell population **(Figure 3F and Supplementary Figure 10)**. These results strongly suggested that case 307 may be benefit from the combined therapy.

Likewise, case 1233 had a *DDR2* amplification in R5, and R5 cells consequently showed sensitivity to dasatinib, an agent known to block over-active DDR2[25, 26], while the unamplified R3, R4 and R6 were dasatinib refractory, even with the ITH low to 12.9% in this case (**Figure 4A**). Accordingly, unamplified PDPCs in case 1233 were screened for potential combination therapy and elesclomol (HSP70 inhibitor) was identified (**Supplementary Figure 11**).

Next, for cases without druggable genomic alterations, mRNA expression of a panel of targetable genes (**Supplementary Table 4**) were evaluated on the multiregional PDPCs to identify cases with heterogeneous expression patterns. Heterogeneous expression of PDGFRA and TOP1 were identified in cases 61 and 703 respectively. For PDGFRA, we applied crenolanib recommended by the MD Anderson Cancer Center (http://pct.mdanderson.org). For TOP1, camptothecin and its derivative irinotecan approved for treating colon cancer by the US-FDA were employed. Similar to the findings in cases 307 and 1233, "biomarker-oriented heterogeneity" (drug target overexpression) determined sensitivity in each subregion (**Figure 4B-C**) despite various ITH (68.5% in case 61 and 36.4% in case 703). Screening the resistant PDPCs in cases

61 and 703 revealed that they were sensitive to YM-155 (Survivin inhibitor) and BMS-754807 (IGF-1R inhibitor) among others respectively (**Supplementary Figure 11**). The current genomic profiling seems difficult to explain the sensitivity of biomarker-absent PDPCs to the agents in our screening, and the underlying mechanisms need further investigation. Nevertheless, this model combining genetic annotations of and pharmacologic testing on multi-regional PDPCs within a tumor allowed us to identify druggable therapeutic strategies.

Comparison of Genetic Profile between PDPCs and Matched Tumor Tissues

To what extent the low-passage PDPCs represent and maintain genomic profiles of original tumors is crucial for their utility. Case 307 with subclonal *FGF19*-amplification was selected for such comparison using WES and CytoScan® HD array. High levels of similarity in mutations and evolutionary architecture between tumor tissues and matched PDPCs were found. There were no significant differences in mutation spectra and mutation types between PDPCs and matched tumor tissues, and mutation shifts toward C>T and C>G substitutions in non-trunk were reproduced in tumor tissues (**Supplementary Figure 12**). In particular, *FGF19* amplification and over 70% (range of 51.3%-91.4%) of the mutations were identical among matched tissues and PDPCs (**Supplementary Figure 13**).

In addition to case 307, the mutations identified from WES data and validated by Sanger sequencing in PDPCs of the remaining cases were recalled by Sanger sequencing in their original tumor regions, if fresh tumor tissues were available. Again, the results showed that 78.2% (range of 50.0%-94.4%) of the mutations were shared by the original

tumor regions and corresponding PDPCs (n=19) (**Supplementary Figure 14A**). Furthermore, to evaluate the genetic stability of our PDPCs, mutations in each case were compared between the 55 PDPCs at early and late passages by Sanger sequencing. Importantly, the results showed that 98.9% (range of 94.0%-100%) of the mutations were shared by the primary cell lines at early and late passages (**Supplementary Figure 14B**). Altogether, although some differences existed, our PDPCs veritably inherited ITH from original tumor tissues and remained genetically stable, and thus may serve as an ideal *in vitro* model to evaluate how ITH affected drug sensitivity.

DISCUSSION

Genomic sequencing has identified several hundred cancer driver alterations across multiple human cancers including HCC.[9, 27] Of note, two deep-sequencing analyses of HCC revealed that 28% of HCCs harbored potentially targetable genetic alterations, with a prevalence of 0.4%-6% for single alteration [8, 13]. The two reports, along with others [9-12], are pivotal to identifying targeted therapies for HCC to achieve better patient prognoses. Further investigating the spatial and temporal genomic heterogeneity in HCC may offer additional insights into therapeutic response, tumor evolutionary history and clinical trial design. Herein, using multi-regional WES on 10 HBV-related HCC, we revealed considerable intratumor heterogeneity in mutational profiles and copy number alterations and a branched evolution in all tumors. Of importance, 53.8% of the driver alterations were revealed to be subclonal events, underscoring the need to refine precision medicine based on cancer driver annotations. Considering that our multi-regional profiling was only conducted on a small fraction of the whole tumor, it is quite possible that even this

study underestimates the true extent of intratumor genetic diversity and subclonal compositions within HCC.

The assumption that different subclones found before therapy may contribute to treatment resistance still needs in-depth validation. Recently, computational modeling has showed that combination drug regimens can maximize tumor-killing effects and minimize the outgrowth of subclones.[28, 29] In this study, we described a patient-derived cell line-based model that enabled direct testing the impact of ITH on therapeutic response. Our data demonstrated that "biomarker-oriented heterogeneity" determined drug sensitivity of each subclone, while additional high-throughput screening of biomarker-absent subclones optimized therapeutic combinations. Thus, our multi-regional PDPC model, integrating genetic and pharmacologic data, may provide an avenue to guide precision cancer therapy. However, potential drug-drug interactions, toxicity interactions, tumor dynamics and tumor microenvironmental regulations may undoubtedly add to the complexity of drug combination optimization. Despite great challenges ahead, we were encouraged by the findings of others suggesting that quick culture of patient or xenograft-derived cancer cells [14, 30, 31] could guide drug discovery to abrogate resistance. Further multi-omic annotations like metabolic, transcriptomic and epigenetic profiling of multi-regional PDPCs will accelerate the discovery of patient-matched drug combinations for better treatment outcomes.

PDPC has previously been used for dissecting genomic landscape of solid tumors due to high tumor cell purity and minimal normal contamination.[32, 33] In this study, the regional PDPCs harbored typical HCC genetic alterations and mutation spectra. Although some differences were evident, PDPCs showed globally similar genetic alterations and

architecture of phylogenetic tree to original tumor tissues. In particular, multi-regional PDPCs maintained substantial genomic heterogeneity and subclonal diversity. Importantly, high-throughput screening on the PDPC model revealed drug response patterns that were not predictable by genetic analysis alone. For an additional example, although FGF19 amplification reciprocates with Wnt/β-catenin signaling activation,[10] the *FGF19*-amplified FGFR4-resistant PDPCs in case 307 showed no responses to GSK3β inhibitors Tideglusib, CHIR-99021 and LY2090314 (data not shown). As such, the data strongly supported that this strategy could provide a comprehensive genetic landscape and simultaneously facilitate the design of combinational treatment strategies.

The optimal therapy should be directed against trunk mutations shared by all subpopulations within a tumor. Such scenario was more likely present in other solid tumors, such as lung (*EGFR* mutation) and breast (HER2 overexpression) cancer, rather than HCC. In this study, the 4 druggable alterations were all located in branches of the phylogenetic tree, implying a subclonal event. Consistently, Schulze et al. [13] reported that druggable genetic alterations, like *FGF3*, *FGF4*, *FGF19* and *CCND1*, appeared at more advanced stages in HCC. Subclonal mutations may become important later in therapy if they enable subclones to resist treatment or confer metastatic capacity. In addition, nearly half of HCC patients harbor multiple lesions, either developed as intrahepatic metastases or as multiple occurrences. Several recent studies comparing the genetic profiles among those multiple lesions within the liver indicated that the presence of multifocal tumors greatly complicated genomic landscape and confounded HCC treatment[34-36]. Collectively, the data may partly explain why targeted therapy has so far been disappointing in HCC.

Currently, genomic profiling has not been integrated into the therapeutic

decision-making and clinical management of HCC patients. ITH adds new levels of complexity in the molecular understanding of HCC, leading to primary and secondary resistance to targeted therapies. Accurate assessment of intratumor genetic heterogeneity based on patient-derived models in HCC is pivotal to design treatment strategies that aim to control resistance.

REFERENCES

1. Ferlay J, Soerjomataram I, Dikshit R, et al. Cancer incidence and mortality worldwide: sources, methods and major patterns in GLOBOCAN 2012. Int J Cancer 2015;136:E359-86.
2. Knox JJ, Cleary SP, Dawson LA. Localized and systemic approaches to treating hepatocellular carcinoma. J Clin Oncol 2015;33:1835-44.
3. Llovet JM, Villanueva A, Lachenmayer A, et al. Advances in targeted therapies for hepatocellular carcinoma in the genomic era. Nat Rev Clin Oncol 2015;12:408-24.
4. Gerlinger M, Rowan AJ, Horswell S, et al. Intratumor heterogeneity and branched evolution revealed by multiregion sequencing. N Engl J Med 2012;366:883-92.
5. Zhang J, Fujimoto J, Wedge DC, et al. Intratumor heterogeneity in localized lung adenocarcinomas delineated by multiregion sequencing. Science 2014;346:256-9.
6. Yates LR, Gerstung M, Knappskog S, et al. Subclonal diversification of primary breast cancer revealed by multiregion sequencing. Nat Med 2015;21:751-9.
7. Sottoriva A, Kang H, Ma Z, et al. A Big Bang model of human colorectal tumor growth. Nat Genet 2015;47:209-16.
8. **Totoki Y, Tatsuno K, Covington KR,** et al. Trans-ancestry mutational landscape of hepatocellular carcinoma genomes. Nat Genet 2014;46:1267-73.
9. Shibata T, Aburatani H. Exploration of liver cancer genomes. Nat Rev Gastroenterol Hepatol 2014;11:340-9.
10. **Ahn SM, Jang SJ, Shim JH,** et al. Genomic portrait of resectable hepatocellular carcinomas: implications of RB1 and FGF19 aberrations for patient stratification. Hepatology 2014;60:1972-82.
11. **Kan Z, Zheng H, Liu X,** et al. Whole-genome sequencing identifies recurrent mutations in hepatocellular carcinoma. Genome Res 2013;23:1422-33.

12. **Guichard C, Amaddeo G, Imbeaud S,** et al. Integrated analysis of somatic mutations and focal copy-number changes identifies key genes and pathways in hepatocellular carcinoma. Nat Genet 2012;44:694-8.
13. **Schulze K, Imbeaud S, Letouze E,** et al. Exome sequencing of hepatocellular carcinomas identifies new mutational signatures and potential therapeutic targets. Nat Genet 2015;47:505-11.
14. Crystal AS, Shaw AT, Sequist LV, et al. Patient-derived models of acquired resistance can identify effective drug combinations for cancer. Science 2014;346:1480-6.
15. Friemel J, Rechsteiner M, Frick L, et al. Intratumor heterogeneity in hepatocellular carcinoma. Clin Cancer Res 2015;21:1951-61.
16. **Nault JC, Calderaro J,** Di Tommaso L, et al. Telomerase reverse transcriptase promoter mutation is an early somatic genetic alteration in the transformation of premalignant nodules in hepatocellular carcinoma on cirrhosis. Hepatology 2014;60:1983-92.
17. Gouas D, Shi H, Hainaut P. The aflatoxin-induced TP53 mutation at codon 249 (R249S): biomarker of exposure, early detection and target for therapy. Cancer Lett 2009;286:29-37.
18. **Sung WK, Zheng H, Li S,** et al. Genome-wide survey of recurrent HBV integration in hepatocellular carcinoma. Nat Genet 2012;44:765-9.
19. Wang Y, Waters J, Leung ML, et al. Clonal evolution in breast cancer revealed by single nucleus genome sequencing. Nature 2014;512:155-60.
20. Swanton C, McGranahan N, Starrett GJ, et al. APOBEC Enzymes: Mutagenic Fuel for Cancer Evolution and Heterogeneity. Cancer Discov 2015;5:704-12.
21. **Imielinski M, Greulich H**, Kaplan B, et al. Oncogenic and sorafenib-sensitive ARAF mutations in lung adenocarcinoma. J Clin Invest 2014;124:1582-6.
22. Horwitz E, Stein I, Andreozzi M, et al. Human and mouse VEGFA-amplified hepatocellular carcinomas are highly sensitive to sorafenib treatment. Cancer Discov 2014;4:730-43.
23. **Arao T, Ueshima K, Matsumoto K,** et al. FGF3/FGF4 amplification and multiple lung metastases in responders to sorafenib in hepatocellular carcinoma. Hepatology 2013;57:1407-15.
24. **Guagnano V, Kauffmann A, Wohrle S,** et al. FGFR genetic alterations predict for sensitivity to NVP-BGJ398, a selective pan-FGFR inhibitor. Cancer Discov 2012;2:1118-33.
25. **Hammerman PS, Sos ML,** Ramos AH, et al. Mutations in the DDR2 kinase gene

identify a novel therapeutic target in squamous cell lung cancer. Cancer Discov 2011;1:78-89.

26. **Bai Y, Kim JY,** Watters JM, et al. Adaptive responses to dasatinib-treated lung squamous cell cancer cells harboring DDR2 mutations. Cancer Res 2014;74:7217-28.
27. MacConaill LE. Existing and emerging technologies for tumor genomic profiling. J Clin Oncol 2013;31:1815-24.
28. Zhao B, Pritchard JR, Lauffenburger DA, et al. Addressing genetic tumor heterogeneity through computationally predictive combination therapy. Cancer Discov 2014;4:166-74.
29. Zhao B, Hemann MT, Lauffenburger DA. Intratumor heterogeneity alters most effective drugs in designed combinations. Proc Natl Acad Sci U S A 2014;111:10773-8.
30. Yu M, Bardia A, Aceto N, et al. Cancer therapy. Ex vivo culture of circulating breast tumor cells for individualized testing of drug susceptibility. Science 2014;345:216-20.
31. **Chen X, Stewart E,** Shelat AA, et al. Targeting oxidative stress in embryonal rhabdomyosarcoma. Cancer Cell 2013;24:710-24.
32. **Stark MS, Woods SL, Gartside MG,** et al. Frequent somatic mutations in MAP3K5 and MAP3K9 in metastatic melanoma identified by exome sequencing. Nat Genet 2012;44:165-9.
33. **Yachida S, Jones S,** Bozic I, et al. Distant metastasis occurs late during the genetic evolution of pancreatic cancer. Nature 2010;467:1114-7.
34. **Xue R, Li R, Guo H,** et al. Variable intra-tumor genomic heterogeneity of multiple lesions in patients with hepatocellular carcinoma. Gastroenterology 2016;150:998-1008.
35. **Shi JY, Xing Q, Duan M**, et al. Inferring the progression of multifocal liver cancer from spatial and temporal genomic heterogeneity. Oncotarget 2016;7:2867-77.
36. **Miao R, Luo H, Zhou H,** et al. Identification of prognostic biomarkers in hepatitis B virus-related hepatocellular carcinoma and stratification by integrative multi-omics analysis. J Hepatol 2014;60:346-53.

Author names in bold designate shared co-first authors.

DATA ACCESS

WES and CytoScan HD array data have been submitted to the European Genome-phenome Archive (https://www.ebi.ac.uk) with the accession number EGAS00001001135.

FIGURE LEGENDS

Figure 1. Spatial and temporal diversity in human HCC revealed by multi-regional deep-sequencing. (**A**) Flowchart of study design. Multiple spatially separated tumor regions were sampled for primary culture. The enriched cancer cells were then subjected to whole-exome sequencing and DNA copy analysis. According to the genomic profiling, biomarker-present cancer cells were treated with predicted compounds, while biomarker-absent cells underwent high-throughput screening for potential precision treatment. (**B**) Phylogenetic trees based on the non-silent mutations. The trunk, branch, and private branch were represented with blue, green and red lines respectively. The evolution distance of each tree was labeled individually, with lengths scaled to the numbers of mutations. Altered driver genes of HCC were mapped to the trunks and branches as indicated. Gene symbols in black, blue and red denote mutations, amplifications and deletions respectively. TERT promoter mutations were detected by Sanger sequencing and were labeled in purple.

Figure 2. Intratumor heterogeneity of somatic mutations and mutation spectrum in human HCC. (**A)** Bar plot showing the ratio of heterogeneous nonsynonymous mutations (number of branch and private branch mutation/number of total mutation) in each tumor, ranging from 12.9%-68.5%. (**B** and **C**) Mutation spectra of nonsynonymous mutations in trunk versus non-trunk (branch and private branch) combined across all 10 cases (**B**) and per case (**C**). Number of mutations was indicated on the top of each bar. The differences between trunk and non-trunk were calculated using χ^2 test. For specific mutation type, Fisher's exact test was used and corrected by Benjamini-Hochberg method where q

values were displayed if $P < 0.05$. (**D)** Hierarchical clustering based on the mutation spectra of trunk and non-trunk of the 10 HCC respectively. Patients were divided into two groups each (I and II as indicated). (**E)** Dot plot showing differences in serum AFP (alpha-fetoprotein) levels between patient groups as indicated in panel **D**. Significant difference was detected in groups I versus II clustered by the spectra of trunk but no non-trunk. NS, not significant.

Figure 3. Combinatorial drug targeting of FGFR-inhibitor sensitive and resistant subclones in case 307. (**A)** Relationship between *FGF19* amplification/overexpression and sensitivity to the pan-FGFR inhibitor. Left panel: Response to the pan-FGFR inhibitor, LY2874455, in all regional PDPCs with or without *FGF19* amplification. Broken line indicates the reference IC50. Middle panel: Relative FGF19 mRNA levels in all regional PDPCs with or without *FGF19* amplification. Arrow indicates regional cells with high expression of FGF19 that were sensitive to LY2874455. Right panel: IC50s to LY2874455 were compared among high, middle and low groups based on mRNA level of FGF19. IC50s in high group were significantly lower than that in other two groups. (**B)** Phylogenetic tree integrating response to LY2874455, *FGF19* amplification and expression in case 307. The biomarker-oriented intratumor heterogeneity, i.e. FGF19 high expression, determined drug response of each subclone. Amp, amplification; exp., expression. (**C**) High FGF19 expression predicted sensitivity to LY2874455 in a panel of HCC cell lines. 105 HCC cell lines were grouped (high versus low/middle) according to their FGF19 mRNA levels, with the cutoff based on the results in case 307. (**D)** Resistant regional PDPCs in case 307 were screened for potential therapeutic combination. Y axis

value was presented as relative IC50 (real IC50/reference IC50). The dots in 6 colors stand for 6 different regions. The red broken line indicates relative IC50=1, dots below which were considered as sensitive. (**E**) Total cell confluence upon the indicated treatment. The confluence of DMSO group on each day was set to 100%. (**F**) Population change of LY2874455 sensitive cells during the indicated treatment. The percentage of LY2874455 sensitive cells in DMSO group on each day was set to 100% (see details in **Supplementary Figure 10**). Error bars: standard deviation. **, P < .01. ***, P < .001.

Figure 4. Personalized drug combinations revealed by biomarker-guided therapeutics and high-throughput screening. Heterogeneous alterations in *DDR2* (**A**), *PDGFRA* (**B**) and *TOP1* (**C**) were detected in cases 1233, 61 and 703 respectively. In each case, the biomarker-present subclones were sensitive to their corresponding compounds (Dasatinib to *DDR2* amplification, Crenolanib to PDGFRA overexpression, and Campthotecin or Irinotecan to TOP1 overexpression), while the biomarker-absent subclones showed resistance. Red broken lines denote the reference IC50s for each indicated compound. Phylogenetic trees integrating drug response and status of biomarkers were drawn for each case. The resistant subclones in each case were high-throughput screened for personalized drug combinations to overcome intratumor heterogeneity, a result not predicted by genetic analysis alone (see details in **Supplementary Figure 9**). Error bars: standard deviation. Amp, amplification; exp., expression.

Figure 1

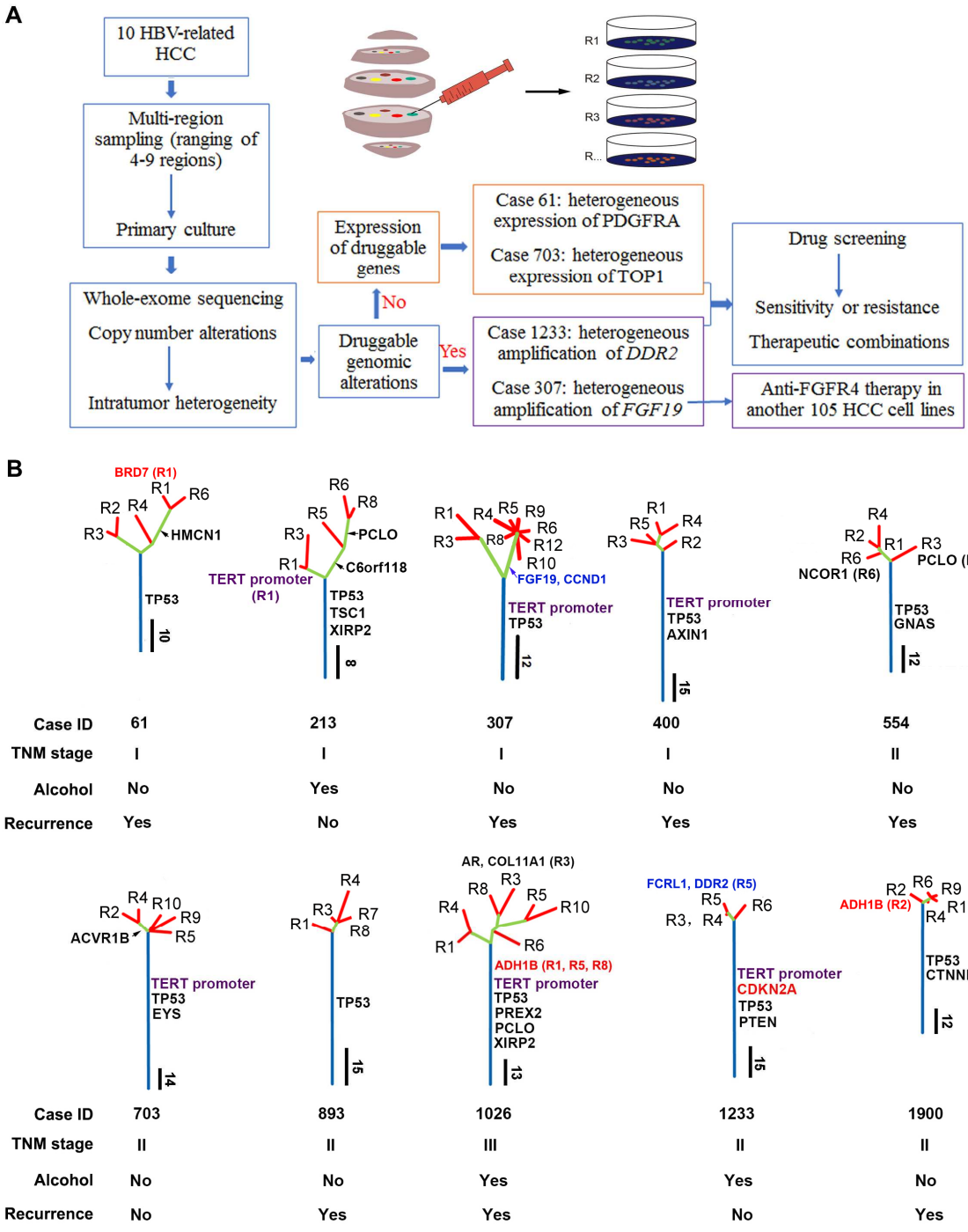
A
10 HBV-related HCC
Multi-region sampling (ranging of 4-9 regions)
Primary culture
Whole-exome sequencing
Copy number alterations
Intratumor heterogeneity
R1
R2
R3
R...
Druggable genomic alterations
No
Yes
Expression of druggable genes
Case 61: heterogeneous expression of PDGFRA
Case 703: heterogeneous expression of TOP1
Case 1233: heterogeneous amplification of DDR2
Case 307: heterogeneous amplification of FGF19
Drug screening
Sensitivity or resistance
Therapeutic combinations
Anti-FGFR4 therapy in another 105 HCC cell lines
B
BRD7 (R1)
HMCN1
TP53
TERT promoter (R1)
PCLO
C6orf118
TP53
TSC1
XIRP2
FGF19, CCND1
TERT promoter
TP53
TERT promoter
TP53
AXIN1
NCOR1 (R6)
PCLO (R3)
TP53
GNAS
Case ID 61 213 307 400 554
TNM stage I I I I II
Alcohol No Yes No No No
Recurrence Yes No Yes Yes Yes
ACVR1B
TERT promoter
TP53
EYS
TP53
AR, COL11A1 (R3)
ADH1B (R1, R5, R8)
TERT promoter
TP53
PREX2
PCLO
XIRP2
FCRL1, DDR2 (R5)
TERT promoter
CDKN2A
TP53
PTEN
ADH1B (R2)
TP53
CTNNB1
Case ID 703 893 1026 1233 1900
TNM stage II II III II II
Alcohol No No Yes Yes No
Recurrence No Yes Yes No Yes

Figure 2

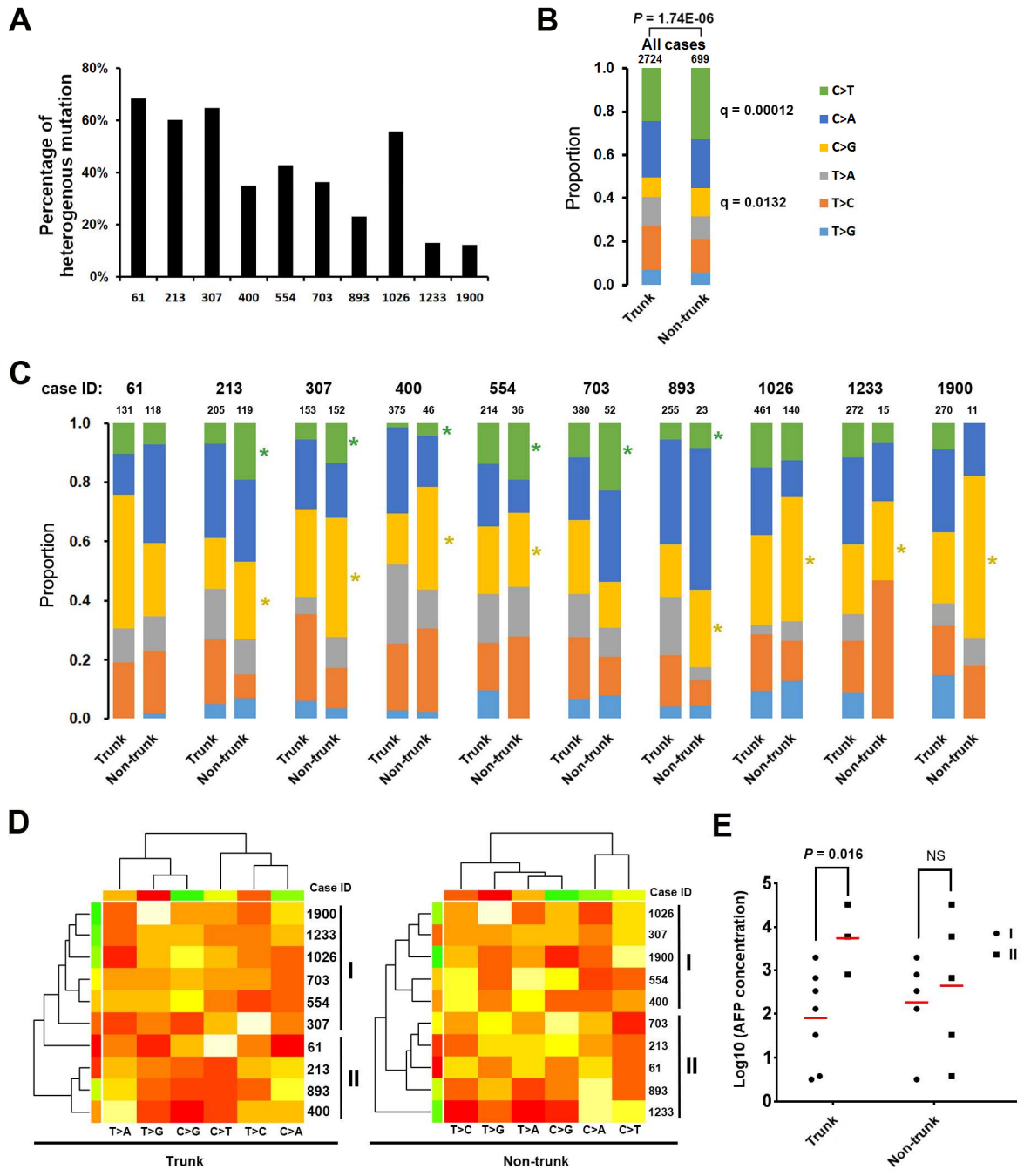
A
Percentage of heterogenous mutation
80%
60%
40%
20%
0%
61 213 307 400 554 703 893 1026 1233 1900
B
P = 1.74E-06
All cases
2724
699
Proportion
q = 0.00012
q = 0.0132
C>T
C>A
C>G
T>A
T>C
T>G
Trunk
Non-trunk
C
case ID: 61 213 307 400 554 703 893 1026 1233 1900
131 118 205 119 153 152 375 46 214 36 380 52 255 23 461 140 272 15 270 11
Proportion
Trunk
Non-trunk
D
Case ID
1900
1233
1026
703
554
307
61
213
893
400
I
II
T>A T>G C>G C>T T>C C>A
Trunk
Case ID
1026
307
1900
554
400
703
213
61
893
1233
I
II
T>C T>G T>A C>G C>A C>T
Non-trunk
E
P = 0.016
NS
Log10 (AFP concentration)
5
4
3
2
1
0
I
II
Trunk
Non-trunk

Figure 3

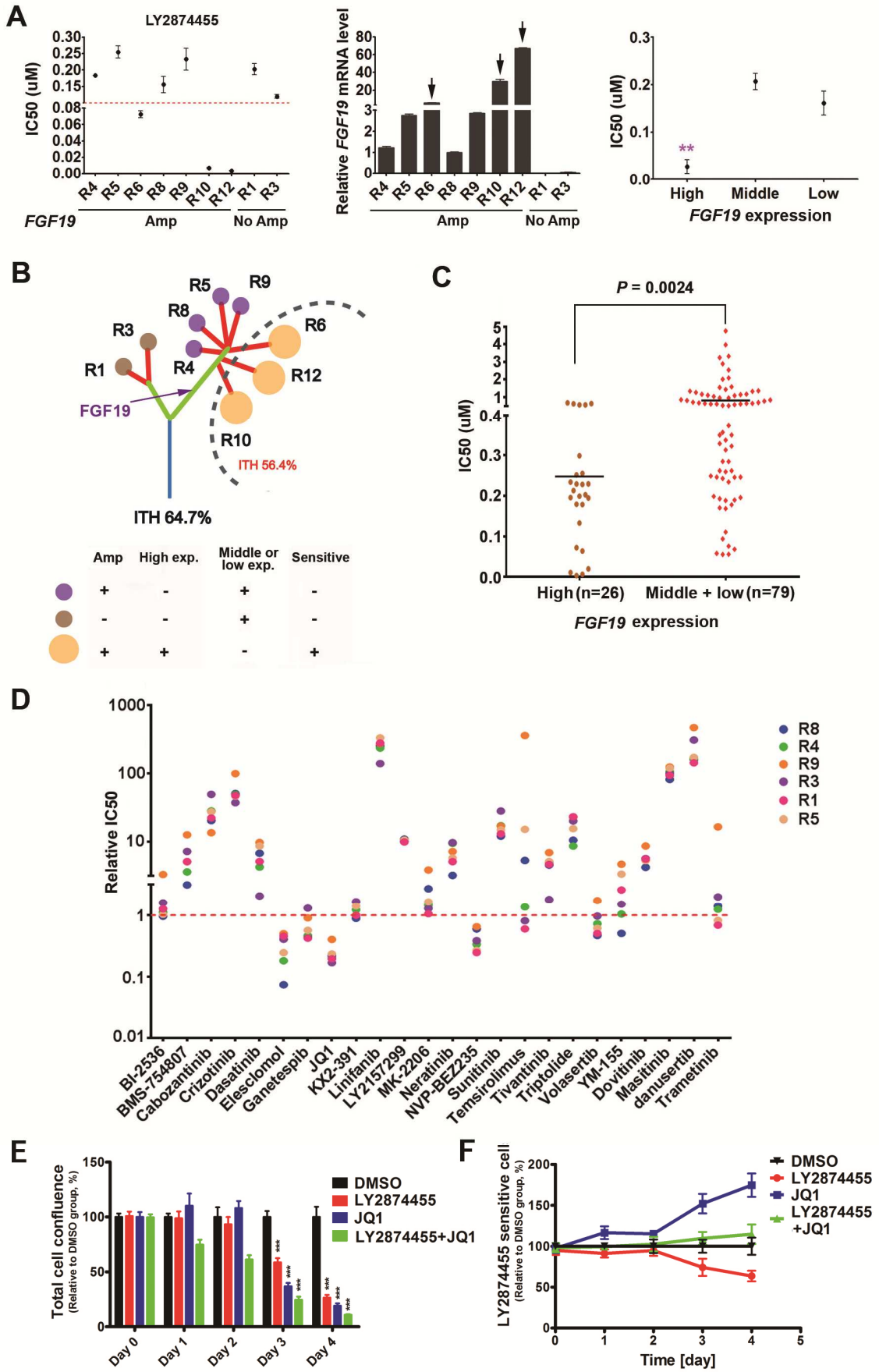
A
LY2874455
IC50 (uM)
R4 R5 R6 R8 R9 R10 R12 R1 R3
FGF19
Amp
No Amp
Relative FGF19 mRNA level
IC50 (uM)
High
Middle
Low
FGF19 expression
B
R5
R9
R8
R3
R6
R1
R4
R12
FGF19
R10
ITH 56.4%
ITH 64.7%
Amp
High exp.
Middle or low exp.
Sensitive
C
P = 0.0024
IC50 (uM)
High (n=26)
Middle + low (n=79)
FGF19 expression
D
Relative IC50
R8
R4
R9
R3
R1
R5
BI-2536
BMS-754807
Cabozantinib
Crizotinib
Dasatinib
Elesclomol
Ganetespib
JQ1
KX2-391
Linifanib
LY2157299
MK-2206
Neratinib
NVP-BEZ235
Sunitinib
Temsirolimus
Tivantinib
Triptolide
Volasertib
YM-155
Dovitinib
Masitinib
danusertib
Trametinib
E
Total cell confluence
(Relative to DMSO group, %)
DMSO
LY2874455
JQ1
LY2874455+JQ1
Day 0
Day 1
Day 2
Day 3
Day 4
F
LY2874455 sensitive cell
(Relative to DMSO group, %)
DMSO
LY2874455
JQ1
LY2874455
+JQ1
Time [day]

Figure 4